Journal of Power Sources 218 (2012) 128–133

Contents lists available at SciVerse ScienceDirect

Journal of Power Sources

journal homepage: www.elsevier.com/locate/jpowsour

Electrochemical properties of $0.6Li[Li_{1/3}Mn_{2/3}]O_2-0.4LiNi_xMn_yCo_{1-x-y}O_2$ cathode materials for lithium-ion batteries

Jun Wang, Bao Qiu, Hailiang Cao, Yonggao Xia*, Zhaoping Liu*

Ningbo Institute of Material Technology & Engineering, Chinese Academy of Sciences, Ningbo 315201, PR China

HIGHLIGHTS

- Li-rich solid solutions have been synthesized by a solid-state reaction method.
- $Li_{1.2}Ni_{0.18}Mn_{0.58}Co_{0.04}O_2$ and $Li_{1.2}Ni_{0.2}Mn_{0.52}Co_{0.08}O_2$ are firstly reported.
- The higher Ni content is, the higher cation mixing is, and the lower resistance is.
- Cation mixing influences capacity, while resistance affects rate capability.

ARTICLE INFO

Article history:
Received 13 March 2012
Received in revised form
15 June 2012
Accepted 19 June 2012
Available online 7 July 2012

Keywords:
Cathode material
Layered lithium-rich
Solid solution
Rate capability

ABSTRACT

Solid solutions between $Li[Li_{1/3}Mn_{2/3}]O_2$ and $LiMO_2$ ($M = Ni_{1/3}Mn_{1/3}Co_{1/3}$, $Ni_{0.4}Mn_{0.4}Co_{0.2}$, $Ni_{0.45}Mn_{0.45}Co_{0.1}$, $Ni_{0.5}Mn_{0.2}Co_{0.3}$, and $Ni_{0.5}Mn_{0.3}Co_{0.2}$) have been synthesized by a solid-state reaction method. The as-prepared $Li_{1.2}Ni_{0.13}Mn_{0.54}Co_{0.13}O_2$, $Li_{1.2}Ni_{0.16}Mn_{0.56}Co_{0.08}O_2$, $Li_{1.2}Ni_{0.18}Mn_{0.58}Co_{0.04}O_2$, $Li_{1.2}Ni_{0.2}Mn_{0.48}Co_{0.12}O_2$, and $Li_{1.2}Ni_{0.2}Mn_{0.52}Co_{0.08}O_2$ solid solutions cathode materials can deliver discharge capacities of 267, 262, 253, 235, and 238 mAh g^{-1}, respectively, at a charge/discharge current density of 25 mA g^{-1} in the voltage range of 2.5–4.7 V. These cathodes all have initial coulombic efficiencies larger than 80%, and show capacity loss less than 0.13% per cycle while cycling at 125 mA g^{-1} for 50 cycles. From Rietveld refinement results and electrochemical impedance spectra (EIS) analysis, it is found that the highest charge/discharge capacity values of $Li_{1.2}Ni_{0.13}Mn_{0.54}Co_{0.13}O_2$ cathode with the lowest Ni content among them are attributed to the lowest cation mixing. While both the $Li_{1.2}Ni_{0.2}Mn_{0.48}Co_{0.12}O_2$ and $Li_{1.2}Ni_{0.2}Mn_{0.52}Co_{0.08}O_2$ cathode materials with higher Ni content exhibit better rate capabilities due to their lower charge transfer resistances and higher electrical conductivities than those of other samples.

1. Introduction

The first report of $Li[Li_xNi_{(1-2x/3)}Mn_{(2-x/3)}]O_2$ by the Dahn group in 2001 has generated worldwide attention to layered Li-rich transition metal oxides nanocomposites [1], either can be regarded as solid solutions of two layered materials, $LiMO_2$ (M = Ni, Mn, and/or Co) and $Li[Li_{1/3}Mn_{2/3}]O_2$ (also can be designated as Li_2MnO_3) [2]. This is attributed to their much higher capacity (>230 mAh g^{-1}) than traditional $LiCoO_2$, $LiNi_{1/3}Mn_{1/3}Co_{1/3}O_2$, $LiMn_2O_4$, and $LiFePO_4$, *etc.* cathode materials [3–5]. However, dramatic capacity fading when cycled at high voltage and poor rate capability are the main obstacles to the application of these cathode materials [6–8].

Over the past decades, much effort has been made to improve the electrochemical performance of layered Li-rich solid solutions. Introduction of cobalt was proven to be an effective way not only to improve crystal structure, but also enhance electrochemical performance [9,10]. Up to now, various Co-doped Li-rich solid solutions between $Li[Li_{1/3}Mn_{2/3}]O_2$ and $LiNi_xMn_yCo_{1-x-y}O_2$, such as $LiNi_{1/3}Mn_{1/3}Co_{1/3}O_2$ [11], $LiNi_{0.5}Mn_{0.2}Co_{0.3}O_2$ [12], $LiNi_{0.375}Mn_{0.375}Co_{0.25}O_2$ [13], $LiNi_{0.4}Mn_{0.4}Co_{0.2}O_2$ [14], $LiNi_{0.1625}Mn_{0.675}Co_{0.1625}O_2$ [15], and $LiNi_{0.4}Mn_{0.5}Co_{0.1}O_2$ [16], *etc.*, have been widely studied. Among these cathode materials, the Li-rich solid solution $0.6Li[Li_{1/3}Mn_{2/3}]O_2-0.4LiNi_{1/3}Mn_{1/3}Co_{1/3}O_2$ ($Li_{1.2}Ni_{0.13}Mn_{0.54}Co_{0.13}O_2$) was the most attractive material in the past several years due to its high discharge capacity [11,17–20]. Recently, more and more researchers have paid attention to $0.6Li[Li_{1/3}Mn_{2/3}]O_2-0.4LiNi_{0.4}Mn_{0.4}Co_{0.2}O_2$ ($Li_{1.2}Ni_{0.16}Mn_{0.56}Co_{0.08}O_2$) material initially for its low cobalt content [14,21]. The $Li_{1.2}Ni_{0.16}Mn_{0.56}Co_{0.08}O_2$ cathode materials exhibit good rate capability [14,21]. The reason for the good rate

* Corresponding authors. Tel./fax: +86 574 86685096.
E-mail addresses: xiayg@nimte.ac.cn (Y. Xia), liuzp@nimte.ac.cn (Z. Liu).

0378-7753/$ – see front matter © 2012 Elsevier B.V. All rights reserved.
http://dx.doi.org/10.1016/j.jpowsour.2012.06.067

Table 1
The experimental (exp.) and theoretical (th.) results of Ni/Co, Mn/Co, and Li/(Ni + Co + Mn) ratios of the five samples.

Sample	Ni/Co		Mn/Co		Li/(Ni + Co + Mn)	
	Exp.	Th.	Exp.	Th.	Exp.	Th.
LR-NMC111	0.994	1.00	0.998	1.00	1.499	1.50
LR-NMC442	1.989	2.00	2.011	2.00	1.504	1.50
LR-NMC992	4.504	4.50	4.999	4.50	1.510	1.50
LR-NMC523	1.668	1.67	0.670	0.67	1.493	1.50
LR-NMC532	2.504	2.50	1.496	1.50	1.492	1.50

capability of less Co content $Li_{1.2}Ni_{0.16}Mn_{0.56}Co_{0.08}O_2$ cathode material leaves us an interesting question, and the solution would find an effective way to enhance rate capability of layered Li-rich solid solution.

In this paper, $0.6Li[Li_{1/3}Mn_{2/3}]O_2$–$0.4LiNi_xMn_yCo_{1-x-y}O_2$ solid solutions were synthesized by a simple solid-state reaction method, using oxalic acid as a precipitant. Among them, both low Co-content $0.6Li_2MnO_3$–$0.4LiNi_{0.45}Mn_{0.45}Co_{0.1}O_2$ and $0.6Li_2MnO_3$–$0.4LiNi_{0.5}Mn_{0.3}Co_{0.2}O_2$ solid solutions were firstly reported. The electrochemical properties, including capacity values, initial coulombic efficiencies, cycling behaviors, and rate capabilities of $0.6Li[Li_{1/3}Mn_{2/3}]O_2$–$0.4LiNi_xMn_yCo_{1-x-y}O_2$ solid solutions were investigated. Moreover, the relationship between structural and electrochemical properties of these samples, especially associating with Ni content at the first time, was discussed in detail.

2. Experimental

2.1. Synthesis

The layered $Li_{1.2}Ni_{0.13}Mn_{0.54}Co_{0.13}O_2$, $Li_{1.2}Ni_{0.16}Mn_{0.56}Co_{0.08}O_2$, $Li_{1.2}Ni_{0.18}Mn_{0.58}Co_{0.04}O_2$, $Li_{1.2}Ni_{0.2}Mn_{0.48}Co_{0.12}O_2$, and $Li_{1.2}Ni_{0.2}Mn_{0.52}Co_{0.08}O_2$ oxides, respectively, which belong to the solid solutions between $Li[Li_{1/3}Mn_{2/3}]O_2$ and $LiNi_{1/3}Mn_{1/3}Co_{1/3}O_2$, $LiNi_{0.4}Mn_{0.4}Co_{0.2}O_2$, $LiNi_{0.45}Mn_{0.45}Co_{0.1}O_2$, $LiNi_{0.5}Mn_{0.2}Co_{0.3}O_2$, and $LiNi_{0.5}Mn_{0.3}Co_{0.2}O_2$, are denoted as LR-NMC111, 442, 992, 523, and 532. The cathode materials were prepared by a solid-state reaction as described below. A stoichiometric amount of lithium hydroxide [$LiOH\cdot H_2O$], nickel acetate [$Ni(CH_3COO)_2\cdot 4H_2O$], manganese acetate [$Mn(CH_3COO)_2\cdot 4H_2O$], cobalt acetate [$Co(CH_3COO)_2\cdot 4H_2O$], and oxalic acid were mixed thoroughly, and calcined by two steps, which were firstly pre-treated at 500 °C for 5 h under air and then calcined at 850 °C for 20 h. Oxalic acid, as a precipitant, is used to produce dry precursor that is easily peeled off from the agate, but not gel material that is hardly handled at room temperature. Besides, it would be beneficial to obtain products with homogenous distribution of transition metal ions. Note that the heating rate was maintained at 5 °C min^{-1}. The samples were cooled with furnace.

2.2. Structure and morphology

Products were characterized by X-ray powder diffraction (XRD, D8 Advance diffractometer, Cu Kα radiation), inductive coupled plasma (ICP, Optima 2100 DV, Perkin–Elmer), and field emission scanning electron microscopy (FESEM, Hitachi S-4800). The specific surface area was measured with a Micromeritics ASAP 2020M instrument. Rietveld refinement was performed on the X-ray diffraction profiles to identify the variation of constants for the unit cell and the collected data were made using the Rietveld Program (*Maud* 2.0). Note that the samples were scanned from $2\theta = 5°$–$110°$ at a low scan rate of 20 s per 0.02°.

2.3. Electrochemical measurements

Electrochemical properties of the LR-NMC111, 442, 992, 523, and 532 electrodes were measured after assembling them into coin cells (type CR2032) in an argon-filled glove box. The cathode was prepared by spreading a mixture of active material (80 wt.%), acetylene black (10 wt.%), and poly (vinylidene fluoride) binder (10 wt.%) dissolved in *N*-methyl pyrrolidone onto an aluminum foil current collector. The cathode was separated from the lithium anode by a separator (Celgard 2502). The electrolyte, consisting of a solution of 1 M $LiPF_6$ in a mixture of ethylene carbonate/dimethyl carbonate (3:7 vol.%), was obtained from Zhangjiagang Guotai-Huarong New Chemical Materials Co., Ltd., PR China. The cells were galvanostatically charged and discharged on a LAND-CT2001A battery test system (Jinnuo Wuhan Co., Ltd., PR China). The electrochemical impedance spectroscopy (EIS) measurements were conducted by Autolab83710 impedance analyzer with an amplitude voltage of 5 mV and frequency range of 0.01 Hz–100,000 Hz. All the EIS tests were performed on the cells after 3-cycles test and rested for 4 h. The fitting of Nyquist plots was performed by the *Zview* 2.0 program. Specific resistance of electrode materials were measured by four point resistivity test system (NAPSON CRESBOX) after coating the cathode slurry on an insulated substrate.

3. Results and discussion

3.1. Structure and morphology

Elemental titration of LR-NMC111, 442, 992, 523, and 532 samples have been evaluated by ICP. The results, reported in Table 1, demonstrate that the synthesis process adopted here provides good

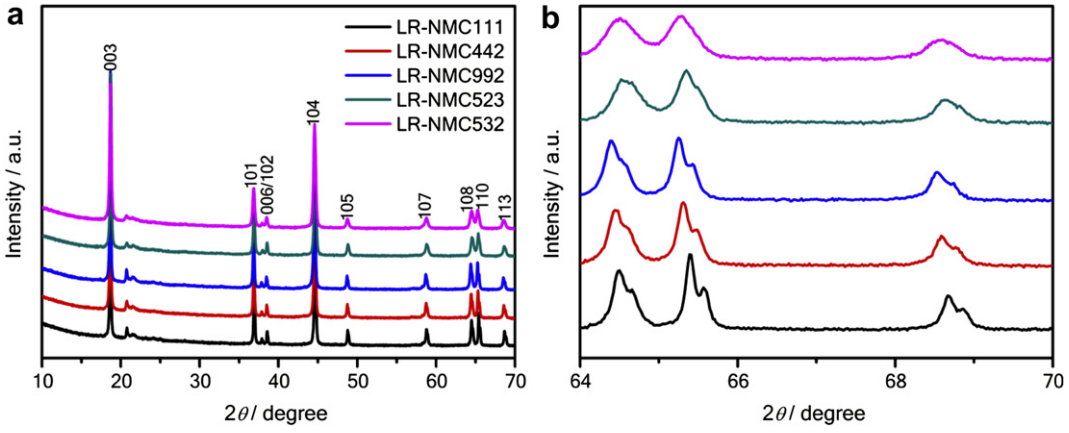

Fig. 1. XRD patterns of LR-NMC111, 442, 992, 523, and 532 samples.

Table 2
The results from Rietveld refinement of the XRD data of the five samples. Note that the structural parameters were denoted to the main phase of *R-3m*.

Sample	a_{hex} (nm)	c_{hex} (nm)	c_{hex}/a_{hex}	R_{wp} (%)	*C2/m* (%)	*R-3m* occupancy: Ni in Li layer (%)
LR-NMC111	0.285127	1.422244	4.9881	4.83	43.1	0.95
LR-NMC442	0.285478	1.423123	4.9851	4.29	50.3	1.00
LR-NMC992	0.285709	1.424135	4.9846	5.08	58.9	1.55
LR-NMC523	0.285365	1.420441	4.9776	3.39	43.9	1.78
LR-NMC532	0.285696	1.421836	4.9767	3.16	45.0	1.73

agreement between theoretical and experimental chemical compositions of the samples, which indicates that the evaporation amount of Li during the calcination is very small.

XRD patterns of the obtained samples were given in Fig. 1. The miller indices of the peaks are demonstrated in the highest panel (Fig. 1a). All the diffraction lines are well indexed as a hexagonal α-$NaFeO_2$ structure (space group: *R-3m*, *NO.* 166), except for a few broad peaks between $2\theta = 20^\circ$ and 25°. The diffraction peaks between $2\theta = 20^\circ$ and 25° correspond to integrated monoclinic Li $[Li_{1/3}Mn_{2/3}]O_2$ phase (*C2/m*), originated from the superlattice ordering of Li and Mn in the transition metal layers for the layered Li-rich oxides [20,22]. As seen in Fig. 1a, both the (006)/(102) and

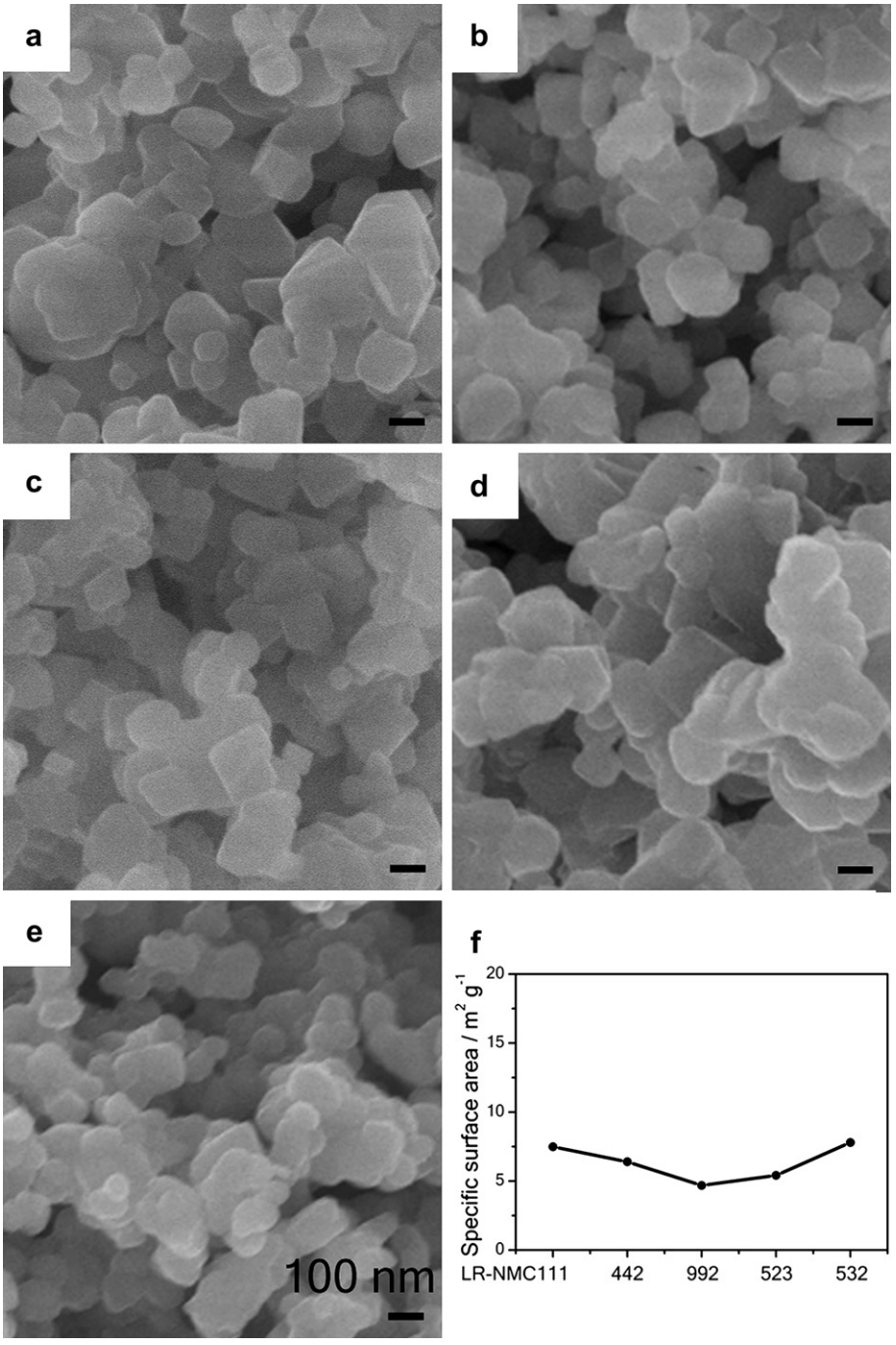

Fig. 2. SEM images of the obtained (a) LR-NMC111, (b) LR-NMC442, (c) LR-NMC992, (d) LR-NMC523, (e) LR-NMC532 samples, and (f) their specific surface area values.

(108)/(110) doublets are well separated, which indicates good hexagonal ordering of the obtained sample [23].

Rietveld refinement was taken to examine the effect of transition metal ratio on the structure of LR-NMC111, 442, 992, 523, and 532 samples. We adopted a software *Maud* 2.0 to perform the refinement based on two structural models (*R-3m* and *C2/m*). The obtained results from Rietveld refinement were listed in Table 2. As can be seen, the difference between the calculated and observed XRD patterns is very small, and all R_w values are smaller than 6%, indicating that the fitting results are good. The value of *c*/*a* is an indicator of the hexagonal ordering, *i.e.*, the higher the *c*/*a*, the better the hexagonal ordering [24]. It can be seen that LR-NMC111 has the highest value of *c*/*a*, followed by LR-NMC 442, 992, 523, and 532 samples. The higher *c*/*a* is, the better hexagonal ordering is.

In the refinement process, we assumed the existence of a small amount of Ni^{2+} in the lithium sites, so called cation mixing, due to small difference in size between the Ni^{2+} (0.69 Å) and Li^+ ions (0.76 Å), in contrast with other cations r(Ni^{3+}) = 0.56 Å, r(Mn^{4+}) = 0.53 Å and r(Co^{3+}) = 0.54 Å [24]. The amounts of Ni in Li layer are 0.95%, 1.00%, 1.55%, 1.78%, and 1.73%, respectively, for LR-NMC111, 442, 992, 523, and 532 samples. It is a conclusion that the higher the *c*/*a*, the better the hexagonal ordering, and the lower the cation mixing, which is consistent with former result [20].

Fig. 1b shows that the splits of (108), (110), and (113) peaks are more and more distinct as Ni content being lower. As is known to all, the high-angle peak spilt is caused by the difference between Kα1 and Kα2, which would occur for high-crystallinity sample. This phenomenon indicates that the sample with higher Ni content has lower crystallinity, which may result from that there are more impure nickel oxides phases or higher cation mixing in the sample with higher Ni content.

As reported before, introduction of cobalt would significantly improve hexagonal ordering and decrease cation mixing [25]. In comparison with the *c*/*a* values and cation-mixing amounts of LR-NMC442/523, 992/523, and 523/532 samples, we can not obtain the similar results. However, it is obvious that the *c*/*a* value and cation-mixing amount show change with the content of Ni. The higher Ni content is, the worse hexagonal ordering is, and the higher cation mixing is. In the following discussion, we will continue to making comparison based on the content of Ni. The relationship between electrochemical performance and structural properties would be discussed in the electrochemical-test section.

The morphology of LR-NMC111, 442, 992, 523, and 532 samples were investigated by scanning electron microscopy, and their specific surface area values were also tested by Brunauer–Emmer–Teller (BET) method, as shown in Fig. 2. It can be seen that the particles of all samples have an average diameter of smaller than 100 nm. There are no big changes of particle size and specific surface area among the samples. As a result, the effects of particle size and specific surface area on the electrochemical properties could be negligible.

3.2. Electrochemical studies

For the purpose of investigation of cathode performance in lithium ion batteries, electrodes were fabricated using the prepared LR-NMC111, 442, 992, 523, and 532 materials and their electrochemical behaviors were evaluated. Fig. 3 shows initial charge/discharge curves of LR-NMC111, 442, 992, 523, and 532 cathodes in the voltage range of 2.5–4.7 V under gravimetric current density of 25 mA g^{-1} (1 C = 250 mA g^{-1}). It is clearly shown that the first charge curves are all accompanied with an irreversible voltage plateau at *ca.* 4.4–4.6 V for oxidation beyond the formal oxidation potential of Ni^{2+} to Ni^{4+} and Co^{3+} to Co^{4+}. The voltage plateau has been assigned to an irreversible loss of oxygen from the lattice as

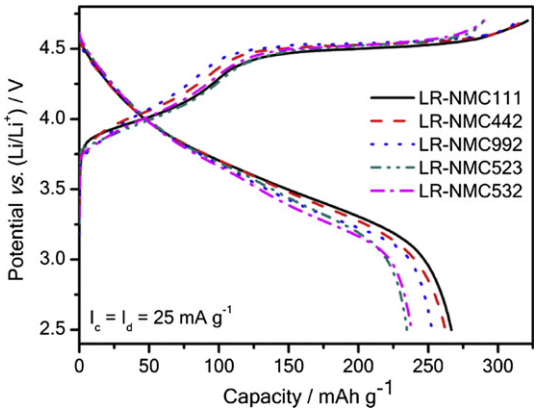

Fig. 3. Initial charge/discharge plots of LR-NMC111, 442, 992, 523, and 532 cathodes under a current density of 25 mA g^{-1}.

revealed by in-situ X-ray diffraction studies [26] and differential electrochemical mass spectroscopy results [27]. During the oxygen loss plateau, the $Li[Li_{1/3}Mn_{2/3}]O_2$ component is activated to form MnO_2 component and thus the material could deliver high discharge capacity during the subsequent discharge process.

As we can see, the obtained LR-NMC111, 442, 992, 523, and 532 cathodes can deliver discharge capacities of 267, 262, 253, 235, and 238 mAh g^{-1}, respectively, with initial coulombic efficiencies of 83.0%, 82.3%, 80.8%, 81.0%, and 82.1%, calculated from the first charge/discharge capacity values as shown in Fig. 3. With the increase of Ni content, the charge/discharge capacity value has a decrease, which is attributed to the higher cation mixing of the sample with higher Ni content, indicated by XRD results. Cation mixing plays an important role in charge/discharge capacity value, which is consistent with former reports [20]. And, here the Ni content or cation mixing does not influence the initial coulombic efficiency. All coulombic efficiencies of the cathodes are higher than common reported values [17,18], which may be attributed to the smaller particle size.

Fig. 4 presents the cycling performance of LR-NMC111, 442, 992, 523, and 532 cathodes at 0.5 C in the voltage range of 2.5–4.7 V. During the extended cycling, LR-NMC111, 442, 992, 523, and 532 cathodes delivered initial capacity values of 200, 204, 196, 190, and 199 mAh g^{-1}, respectively, and have capacity retentions of 99.4%, 93.8%, 93.4%, 99.7%, and 97.4% after 50 cycles. Each capacity loss value is no more than 0.13% per cycle, showing the good cycling performance of all cathodes. In contrast, the transition metal ratio does not obviously effect on the cycling performance of layered Li-rich materials. Hong et al. reported the synthesis of $Li[Li_xNi_{(1-2x/3)}Mn_{(2-x/3)}]O_2$ materials by a combustion method, however, there was a significant capacity loss of several tens of cycles [6]. Similar problems were also observed in other layered Li-rich solid solutions [17,18]. Here, it is believed that the use of oxalic acid resulted in homogeneous distribution of transition metal ions in all prepared cathode materials, thereby high capacity retentions.

The rate capability is an important factor for battery performance. To compare the rate capabilities of LR-NMC111, 442, 992, 523, and 532 cathodes, all coin cells were galvanostatically charged at 0.1 C and discharged at different C-rates from 0.1 C to 2 C rates in the voltage range of 2.5–4.7 V. The normalized discharge capacity values are shown in Fig. 5a. It is obvious that the rate capability of LR-NMC532 cathode is the best among them, and then LR-NMC992, followed by LR-NMC442, and the worst is LR-NMC111. Note that the rate capability of LR-NMC523 cathode keeps nearly identical with LR-NMC532, regardless of the various C rates. The real discharge capacity values at various C rates were also given in Fig. 5b. As can

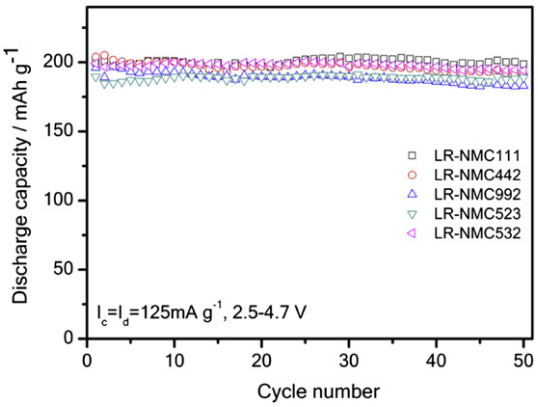

Fig. 4. Cycling performance of LR-NMC111, 442, 992, 523, and 532 cathodes under 125 mA g^{-1} in the voltage range of 2.5–4.7 V.

be seen, both LR-NMC523 and 532 cathodes can deliver discharge capacity values around 170 mAh g^{-1} at 2C, while LR-NMC141 only has a discharge capacity of 110 mAh g^{-1}, which corresponds to the above result, *i.e.*, the rate capability of Li-rich cathode has been significant improved as the Ni content increasing. However, XRD results showed that the cation mixing became larger with the increase of Ni content. The large cation mixing would deteriorate cell performance. Here, it is possible that another more important factor influence rate capability of the cathode material. In some case, rigid crystal structure can not accommodate fast Li^+ ions diffusion, while less crystallized or amorphous structure can. As indicated by above XRD results, the samples with higher Ni content exhibit lower crystallinity due to higher cation mixing or more impure phases. Hence, the lower crystallinity of the samples with

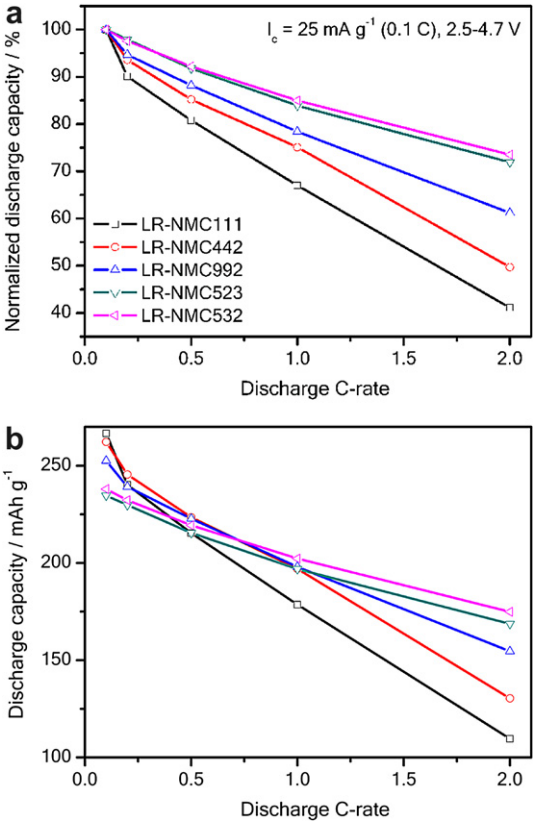

Fig. 5. Normalized discharge capacity values of LR-NMC111, 442, 992, 523, and 532 cathodes at various C rates.

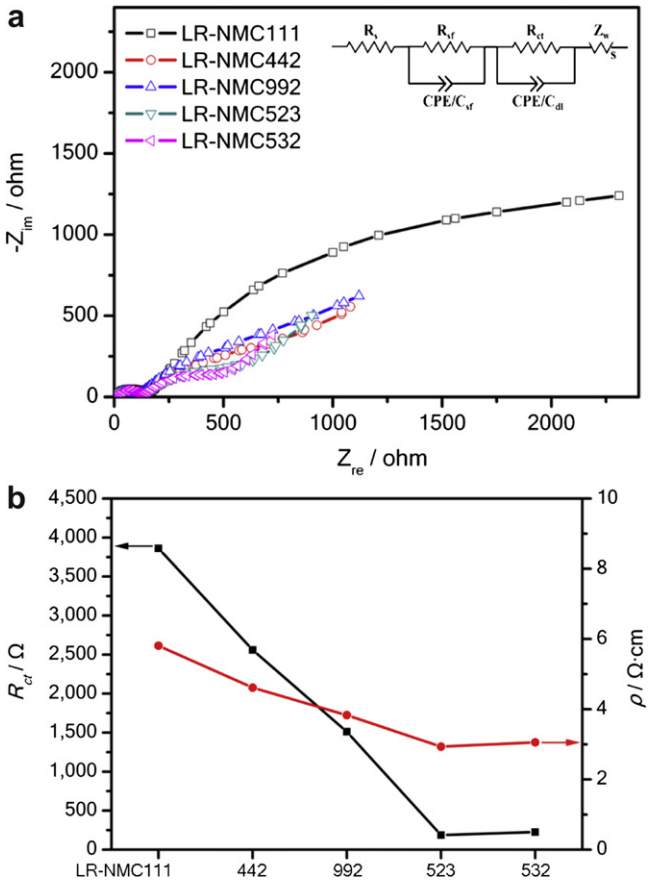

Fig. 6. (a) Electrochemical impedance Nyquist diagrams (Z_{re} *vs.* $-Z_{im}$), and (b) charge transfer/specific resistances of LR-NMC111, 442, 992, 523, and 532 cathodes. The insert: the equivalent circuit adopted to fit impedance spectra.

higher Ni content may be responsible for their better rate capabilities.

In order to reveal the intrinsic reason of such phenomenon, the EIS tests were performed on the LR-NMC111, 442, 992, 523, and 532 cathodes after 3-cycles test at 0.1 C and rested for 4 h. The electrochemical Nyquist diagrams are shown in Fig. 6a. The inset of Fig. 6a shows the equivalent circuit to model the Nyquist plots. In this equivalent circuit, R_s represents the internal resistance of the battery. R_{sl} and *CPE1* represent the resistance and capacitance of the SEI film. R_{ct} and *CPE2* are corresponding to the charge-transfer resistance and double-layer capacitance. Z_W is the Warburg impedance related to Li^+ ions diffusion [28]. The fitted impedance parameters are plotted in Fig. 6b. It can be seen from Fig. 6b that both the R_{ct} values for the LR-NMC523 and 532 cathodes are much lower than those of other cathodes. Moreover, the four probe tests also show that the cathodes of LR-NMC523 and 532 have specific resistances lowering than the others (Fig. 6b). In deed, observing colors of the obtained LR-NMC111, 442, 992, 523, and 532 materials, we found that the samples exhibited a trend of being darker as Ni content increasing. Overall, the results indicate that both the LR-NMC523 and 532 cathodes have lower charge-transfer resistances and higher electrical conductivities (lower specific resistances), thereby exhibit higher rate capabilities as mentioned above.

4. Conclusions

Layered $Li_{1.2}Ni_{0.13}Mn_{0.54}Co_{0.13}O_2$, $Li_{1.2}Ni_{0.16}Mn_{0.56}Co_{0.08}O_2$, $Li_{1.2}Ni_{0.18}Mn_{0.58}Co_{0.04}O_2$, $Li_{1.2}Ni_{0.2}Mn_{0.48}Co_{0.12}O_2$, and $Li_{1.2}Ni_{0.2}Mn_{0.52}Co_{0.08}O_2$ cathode materials have been successfully prepared

through a solid-state reaction method. It is the use of oxalic acid that results in homogeneous distribution of transition metal ions in all prepared cathode materials, thereby high capacity retentions. The higher Ni content is, the higher cation mixing is, and the lower charge transfer resistance is. The cation mixing influences charge/discharge capacity value, while the charge transfer resistance or electrical conductivity affects rate capability. Both initial coulombic efficiency and cycling performance do not vary with different transition metal ratio. Hence, $Li_{1.2}Ni_{0.13}Mn_{0.54}Co_{0.13}O_2$ cathode is more applicable in high-energy storage device, and $Li_{1.2}Ni_{0.2}Mn_{0.52}Co_{0.08}O_2$ cathode could be applied in electric vehicle with high-power capability. The work about further decrease/increase of Ni content in layered Li-rich cathodes is in progress.

Acknowledgements

We are grateful for financial support from the Chinese Academy of Sciences (Program of Knowledge Innovation), the Natural Science Foundation of Ningbo (Grant No. 2011A610201 and 2010A610150), Zhejiang Provincial Natural Science Foundation of China (Grant No. R4100194 and Y4100499).

References

[1] Z.H. Lu, D.D. MacNeil, J.R. Dahn, Electrochem. Solid-State Lett. 4 (2001) A191–A194.
[2] M.M. Thackeray, C.S. Johnson, J.T. Vaughey, N. Li, S.A. Hackney, J. Mater. Chem. 15 (2005) 2257–2267.
[3] Z.H. Lu, L.Y. Beaulieu, R.A. Donaberger, C.L. Thomas, J.R. Danh, J. Electronchem. Soc. 149 (2002) A778–A791.
[4] D.K. Lee, S.H. Park, K. Amine, H.J. Bang, J. Parakash, Y.K. Sun, J. Power Sources 162 (2006) 1346–1350.
[5] M.M. Thackeray, S.H. Kang, C.S. Johnson, J.T. Vaughey, R. Benedek, S.A. Hackney, J. Mater. Chem. 17 (2007) 3112–3125.
[6] Y.S. Hong, Y.J. Park, K.S. Ryu, S.H. Chang, M.G. Kim, J. Mater. Chem. 14 (2004) 1424–1429.
[7] H.X. Deng, I. Belharouak, Y.K. Sun, K. Amine, J. Mater. Chem. 19 (2009) 4510–4516.
[8] T. Ohzuku, M. Nagayama, K. Tsuji, K. Ariyoshi, J. Mater. Chem. 21 (2011) 10179–10188.
[9] L.Q. Zhang, K. Takada, N. Ohta, K. Fukuda, T. Sasaki, J. Power Sources 146 (2005) 598–601.
[10] I. Belharouak, G.M. Koenig Jr., J.W. Ma, D.P. Wang, K. Amine, Electrochem. Commun. 13 (2011) 232–236.
[11] J.M. Zheng, X.B. Wu, Y. Yang, Electrochim. Acta 56 (2011) 3071–3078.
[12] J.H. Park, J. Lim, J. Yoon, K.S. Park, J. Gim, J. Song, H. Park, D. Im, M. Park, D. Ahn, Y. Paik, J. Kim, Dalton Trans. 41 (2012) 3053–3059.
[13] S. Sivaprakash, S.B. Majumder, J. Electrochem. Soc. 157 (2010) A418–A422.
[14] J. Li, R. Klopsch, M.C. Stan, S. Nowak, M. Kunze, M. Winter, S. Passerini, J. Power Sources 196 (2011) 4821–4825.
[15] W.C. West, J. Soler, M.C. Smart, B.V. Ratnakumar, S. Firdosy, V. Ravi, M.S. Anderson, J. Hrbacek, E.S. Lee, A. Manthiram, J. Electrochem. Soc. 158 (2011) A883–A889.
[16] J.H. Jeong, B.S. Jin, W.S. Kim, G.X. Wang, H.S. Kim, J. Power Sources 196 (2011) 3439–3442.
[17] J. Gao, A. Manthiram, J. Power Sources 191 (2009) 644–647.
[18] J. Gao, J. Kim, A. Manthiram, Electrochem. Commun. 11 (2009) 81–84.
[19] N. Yabuuchi, K. Yoshii, S.T. Myung, I. Nakai, S. Komaba, J. Am. Chem. Soc. 133 (2011) 4404–4419.
[20] J. Wang, G.X. Yuan, M.H. Zhang, B. Qiu, Y.G. Xia, Z.P. Liu, Electrochim. Acta 66 (2012) 61–66.
[21] H.J. Kim, H.G. Jung, B. Scrosati, Y.K. Sun, J. Power Sources 203 (2012) 115–120.
[22] J. Wang, X.Y. Yao, X.F. Zhou, Z.P. Liu, J. Mater. Chem. 21 (2011) 2544–2549.
[23] J.R. Dahn, U.V. Sacken, C.A. Michal, Solid State Ionics 44 (1990) 87–97.
[24] X.Y. Zhang, W.J. Jiang, A. Mauger, Q. Lu, F. Gendron, C.M. Julien, J. Power Sources 195 (2010) 1292–1301.
[25] C. Nithya, R. Thirunakaran, A. Sivashanmugam, G.V.M. Kiruthika, S. Gopukumar, J. Phys. Chem. C 113 (2009) 17936–19744.
[26] R. Armstrong, M. Holzapfel, P. Novak, C.S. Johnson, S.H. Kang, M.M. Thackeray, P.G. Bruce, J. Am. Chem. Soc. 128 (2006) 8694–8698.
[27] Z.H. Lu, J.R. Danh, J. Electronchem. Soc. 149 (2002) A815–A822.
[28] Z. Li, F. Du, X.F. Bie, D. Zhang, Y.M. Cai, X.R. Cui, C.Z. Wang, G. Chen, Y.J. Wei, J. Phys. Chem. C 114 (2010) 22751–22757.